Energy Proceedings
Vol 53, 2025
ISSN 2004-2965

Data-driven dimensional analysis of flow boiling critical heat flux in microgravity#

Kuang Yang, Zhicheng Liang, Yunhao Zhang, Xinying Wang, Qiang Li, Haijun Wang*

State Key Laboratory of Multiphase Flow in Power Engineering, Xi'an Jiaotong University, Xi'an 710049, China

(*Haijun Wang: whj@mail.xjtu.edu.cn)

ABSTRACT

Energy management in deep space exploration poses significant challenges for the stable and safe operation of thermal management systems. The critical heat flux (CHF) in flow boiling, as a key safety threshold for two-phase heat transfer systems, must be thoroughly investigated. The current work introduces a data-driven dimensional analysis method that can automatically discover characteristic dimensionless numbers from physical data. This approach addresses the issues of non-uniqueness and the inability to measure the importance of results inherent in the classic Buckingham Pi theorem. By collecting CHF datasets of different fluid media under both Earth's gravity and space microgravity conditions in vertical tubes, the algorithm identified the most influential dimensionless number affecting the boiling number Bo_{chf} during boiling crises and determined the corresponding exponential scaling relationship. This led to the development of a new CHF predictive correlation applicable across different fluids and conditions. Comparison results with several other models indicate that the proposed correlation offers higher accuracy and can potentially be used in the design and optimization of high-power thermal management systems for space, lunar, and Martian environments.

Keywords: microgravity, critical heat flux, data-driven dimensional analysis, scaling law

NONMENCLATURE

Abbreviations	
CHF	Critical heat flux
GELU	Gaussian error linear units
MAE	Mean absolute error
MAPE	Mean absolute percentage error
MLP	Multilayer perceptron
MSE	Mean squared error
Symbols	
Bo	Boiling number
Bd	Bond number
DR	Density ratio
g	Gravity acceleration [m / s^2]
G	Mass flux [kg / m^{2}s]
L_h	Tube heated length [m]
KR	Kinetic energy to phase change energy ratio
Pr	Prandtl number
q''	Heat flux [W / m^2]
Re	Reynolds number
We	Weber number
π	Dimensionless number
α	Thermal diffusivity [m^2 / s]
μ	Dynamic viscosity [Pa s]
ρ	Density [kg / m^3]
σ	Surface tension coefficient [N / m]

1. INTRODUCTION

The ambitious goals of deep space exploration, characterized by increasing distances and mission durations, pose significant challenges to the stable power supply of spacecraft [1]. Given the limited payload and space constraints of cosmic missions, there is a critical need for highly energy-efficient thermal exchange systems. Flow boiling heat transfer, renowned for its high heat transfer coefficients, is considered a promising technological pathway for space heat exchangers. To ensure the safe and efficient application of flow boiling heat transfer in space, it is imperative to thoroughly investigate the critical heat flux (CHF) under microgravity conditions. This is essential to avoid the severe decline in heat transfer coefficient and the abrupt rise in wall temperature that occurs when the CHF is exceeded.

Space missions, from orbital to lunar to Martian, operate under varying gravitational conditions, ranging from microgravity (μg) to 0.17g and 0.38g, respectively. These conditions differ significantly from Earth's gravity, resulting in distinct buoyancy effects that impact flow, heat, and mass transfer processes. Numerous experiments conducted in orbit, drop tower microgravity experiments, and aircraft parabolic flight tests have demonstrated that the CHF of flow boiling under microgravity conditions differs from that under normal gravity. This underscores the necessity for new predictive tools tailored to microgravity environments.

Current methods for predicting the CHF of flow boiling primarily include mechanistic models [2] and

This is a paper for the 16th International Conference on Applied Energy (ICAE2024), Sep. 1-5, 2024, Niigata, Japan.

empirical correlations [3]. Mechanistic models rely on theoretical assumptions and phenomenological analyses of high-resolution experiments, such as simplifying assumptions about liquid films and bubble shapes based on high-speed imaging results. These models are highly dependent on the researcher's expertise and are often costly, especially under microgravity conditions. Moreover, most mechanistic models have not been validated for microgravity conditions, limiting their applicability. Empirical correlation methods, on the other hand, depend on the Buckingham Pi theorem [4] to select dimensionless variables and fit the relevant correlations. Both methods partly rely on heuristic approaches, such as trial-and-error methods, which struggle to provide optimal solutions for complex multi-parameter problems. Therefore, there is a pressing need for more robust and accurate predictive models that rely less on empirical assumptions and more on data-driven insights.

Advancements in data science offer new potential solutions for complex engineering and physical problems. Constantine et al. [5] proposed a data-driven dimensional analysis algorithm that combines the Buckingham Pi theorem with the active subspace method, enabling the automatic discovery of the most influential dimensionless numbers from high-dimensional data. This approach addresses previous issues related to the non-uniqueness and importance quantification of dimensionless numbers in the application of the Buckingham Pi theorem. The success of this method in various fields highlights its potential for addressing complex problems in heat transfer and fluid dynamics. For instance, Jofre et al. [6] identified the dominant dimensionless numbers in heat transfer in irradiated particle-laden turbulent flow using data-driven methods. Similarly, Hang et al. [7] applied this approach to the dynamics in a 3D print molten pool, while Xu et al. [8] and Zhang et al. [9] further combined this method with neural networks and clustering algorithms, applying it to the dimensional analysis of drag coefficients of a flexible body and the spread of oil slicks on a calm sea.

Building on these advancements, the current work analyzes the CHF of flow boiling under microgravity conditions using a data-driven dimensional analysis algorithm. By identifying the dominant dimensionless numbers and corresponding scaling laws, a new dimensionless predictive model is developed. This model not only addresses the limitations of existing predictive methods but also demonstrates superior accuracy compared to other relevant correlations. This innovative approach offers a promising advancement in the predictive modeling of flow boiling CHF in microgravity, potentially contributing to the broader goal of enhancing efficient and safe thermal management in deep space missions.

2. DATA-DRIVEN DIMENSIONAL ANALYSIS

2.1 Methodology

According to the Buckingham Pi theorem, a dimensionless dependent variable *Y* can be expressed in terms of at most $n = m - k$ dimensionless numbers of m dimensional variables with *k* dimensions $\boldsymbol{q} = [q_1, q_2, \ldots, q_n]$:

$$\begin{aligned} Y &= f(\boldsymbol{q}) \\ &= g\left[\boldsymbol{W}^T \log(\boldsymbol{q})\right] \\ &= g(\boldsymbol{x}) \end{aligned} \tag{1}$$

Here, $\boldsymbol{x}$ represents the dimensionless numbers after applying the logarithm operation, and $\boldsymbol{W}$ is the matrix of exponents for the dimensionless numbers, determined by dimensional homogeneity from the null space of the following homogeneous linear equation system:

$$\boldsymbol{DW} = \boldsymbol{0}_{k\times n} \tag{2}$$

The matrix $\boldsymbol{D}$ is a $k \times m$ dimensional matrix, where each row corresponds to a dimension and each column corresponds to a unit of a physical quantity. For instance, if the dimensions from top to bottom are length, mass, and time, the column for density would be represented as $[-3, 1, 0]^T$.

Upon obtaining $\boldsymbol{W}$, a dimensionless representation of $\boldsymbol{x}$ is derived; however, this representation may not be the most suitable for the problem at hand. The active subspace method is employed to analyze the sensitivity of the dimensionless variable x with respect to *Y*, i.e., gradient analysis. For the function $Y = g(\boldsymbol{x})$, the following covariance matrix can be computed and eigenvalue decomposition performed:

$$\begin{aligned} \boldsymbol{C} &= \int \nabla g(\boldsymbol{x}) \nabla g^T(\boldsymbol{x}) d\boldsymbol{x} \\ &= \boldsymbol{S\Lambda S}^T \end{aligned} \tag{3}$$

Each column of matrix $\boldsymbol{S}$ represents the principal directions of variation in g, with the corresponding eigenvalues $\boldsymbol{\Lambda}$ indicate the extent of variation. Based on the decomposed eigenvector matrix, a new dimensionless representation can be obtained:

$$\boldsymbol{Z} = \boldsymbol{WS} \tag{4}$$

The matrix $\boldsymbol{Z}$ satisfies the dimensional homogeneity equation $\boldsymbol{DZ} = 0$, where each column represents a dimensionless number and each element denotes the exponent of a physical quantity. Furthermore, from left to right, each column represents dimensionless numbers with decreasing influence on Y. The first column of the matrix indicates the dominant dimensionless number, to which Y is most sensitive.

In the context of a given dataset, the data-driven dimensional analysis algorithmic workflow illustrated in Fig. 1 is employed to identify the aforementioned dominant dimensionless numbers.

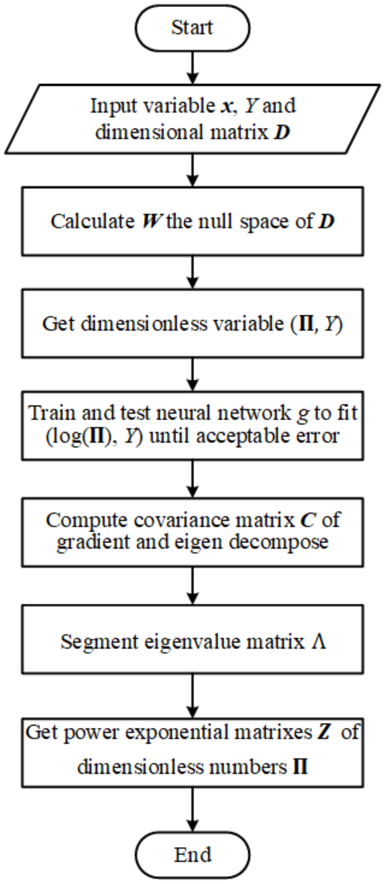

Fig 1 Algorithm of the data-driven dimensional analysis

2.2 Dataset description

Data from both microgravity [10-13] and Earth's gravity [14-18] environments are utilized to uncover unified physical laws for potential applications in varying gravity conditions such as those found in space, on the Moon, and on Mars.

The microgravity dataset comprises 135 data points of FC-72 fluid under microgravity conditions on the International Space Station, collected from five sources, as detailed in Table 1. To ensure accuracy, only data values provided in tables or text are included, excluding coordinate data extracted from images. The microgravity dataset features a hydraulic diameter of 3.33 mm, a heating length of 1148 mm, pressure ranges from 121.16 to 182.79 kPa, inlet thermodynamic quality from −0.53 to 0.50, and mass flux from 180.04 to 3200 kg/m²s. For Earth's gravity conditions, the study uses 24 vertical flow CHF data points of FC-72 fluid from four sources and a publicly available dataset of 1438 data points of water fluid vertical tube flow processed by Yang et al. [19] (initially published by Zhao et al. [14]). The Earth's gravity FC-72 data have a hydraulic diameter of 3.33 mm, a heating length of 1148 mm, pressure ranges from 115.80 to 191.20 kPa, inlet thermodynamic quality from −0.41 to 0.52, and mass flux from 190.8 to 3200 kg/m²s.

Table 1 Data source

Author (year)	Gravity condition	Fluid	Channel Geometry	#.
Mudawar et al. [11] (2023)	μg ($\approx 10^{-6} g_e$)	FC-72	Rectangle	36
Mudawar et al. [12] (2023)	μg ($\approx 10^{-6} g_e$)	FC-72	Rectangle	26
Mudawar et al. [10] (2023)	μg ($\approx 10^{-6} g_e$)	FC-72	Rectangle	46
Mudawar et al. [13] (2024)	μg ($\approx 10^{-6} g_e$)	FC-72	Rectangle	27
O'Neill et al. [15] (2018)	g_e	FC-72	Rectangle	4
Devahdhanush et al. [17] (2022)	g_e	FC-72	Rectangle	9
Darges et al. [16] (2022)	g_e	FC-72	Rectangle	2
Devahdhanush et al. (2022)	g_e	FC-72	Rectangle	9
Zhao et al. [14] (2020)	g_e	Water	Circle	1438
All				1597

The physical parameters and properties within the dataset are employed to predict the boiling number representing the CHF, denoted as $Bo_{chf} = q''_{chf} / Gh_{fg}$. Through data-driven dimensional analysis, the most influential dimensionless variable affecting Bo_{chf} is identified. The dimensional physical quantities used as inputs can be categorized as follows:

(1) Geometric Parameters: hydraulic diameter d, equivalent heated diameter d_h and heated length L_h.

(2) Material properties: saturated liquid density ρ_f, saturated vapor density ρ_g, density difference $\Delta\rho = \rho_f - \rho_g$, saturated liquid viscosity μ_f, latent heat h_{fg}, thermal diffusivity of saturated liquid α_f, and surface tension coefficient σ.

(3) Thermodynamic state: Enthalpy difference between the saturated vapor and inlet condition $\Delta h = h_{sat,g} - h_{in}$.

(4) Flow Parameters: mass flux G and gravitational acceleration g.

The dimensional matrix for these input variables is shown in Eq. (5), where $\boldsymbol{D}$ is utilized to compute a null space $\boldsymbol{W}$, which reduces the dimensionality of the 13 dimensional variables to 10 dimensionless numbers.

$$\boldsymbol{D}=\begin{bmatrix} 1 & 1 & 1 & -3 & -3 & -3 & -1 & 2 & 2 & 2 & 0 & -2 & 1 \\ 0 & 0 & 0 & 1 & 1 & 1 & 1 & 0 & 0 & 0 & 1 & 1 & 0 \\ 0 & 0 & 0 & 0 & 0 & 0 & -1 & -2 & -2 & -1 & -2 & -1 & -2 \end{bmatrix}\begin{matrix} M(\mathrm{kg}) \\ T(\mathrm{s}) \\ \Theta(\mathrm{K}) \end{matrix} \tag{5}$$

2.3 *Neural network structure and training process*

A multilayer perceptron (MLP) neural network is employed to fit the mapping relationship between the 14 dimensionless inputs and Bo_{chf}. The network comprises an input layer, hidden layers with node counts of [32, 64, 64, 32], and a linear output layer. The activation function used is the Gaussian Error Linear Unit (GELU) [20], which is expressed as:

$$\mathrm{GELU}(x)=\frac{x}{2}\left[1+\mathrm{erf}\left(\frac{x}{\sqrt{2}}\right)\right] \tag{6}$$

where erf(·) is the Gauss error function.

The loss function for network is defined as the mean squared error (*MSE*) with the dimensionless dependent variable Bo_{chf}, as shown below:

$$MSE\left(Bo_{\mathrm{pre}}\right)=\frac{1}{N}\sum_{i=1}^{N}\left(Bo_{\mathrm{pre}}-Bo_{\mathrm{true}}\right)^2 \tag{7}$$

Here, the subscripts "pre" and "true" represent the network's predicted and true values from the dataset, respectively.

To ensure an accurate evaluation of the network's fitting capabilities and to prevent overfitting, 20% of the data is randomly selected as a validation set during the network training phase. This training/validation split is consistently maintained throughout all stages to avoid data leakage. The network parameters are updated using the Adam [21] optimization algorithm, known for its efficiency in achieving rapid convergence. The learning rate is set at 1×10^{-3}, and the weight decay is configured at 1×10^{-7}. Each training epoch utilizes the entire training set as input, adopting a full batch size approach. The networks undergo training for a total of 10,000 epochs.

3. RESULTS

3.1 *Dominating dimensionless number and correlation*

Based on the algorithm described in Section 2.1, a set of dimensionless representations and the eigenvalues representing the influence of different dimensionless numbers were obtained, as shown in Fig. 2. It can be observed that the first eigenvalue is significantly larger than the subsequent values, indicating that the dependent variable Bo_{chf} can be well represented by a single dominant dimensionless number. The dominant first dimensionless number is as follows (with exponents retained to three decimal places):

$$\pi=\frac{d^{0.138}\rho_{\mathrm{g}}^{0.105}\Delta h^{0.397}\sigma^{0.460}g^{0.008}}{d_{\mathrm{h}}^{0.072}L_{\mathrm{h}}^{0.121}\rho_{\mathrm{f}}^{0.075}\Delta\rho_{\mathrm{b}}^{0.265}\mu_{\mathrm{f}}^{0.014}h_{\mathrm{fg}}^{0.561}\alpha_{\mathrm{f}}^{0.382}G^{0.211}} \tag{8}$$

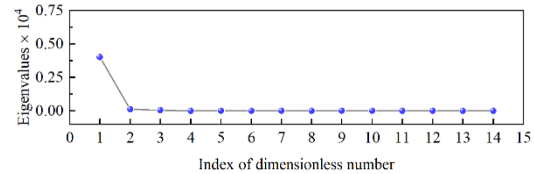

Fig 2 Eigenvalues of discovered dimensionless numbers

The data for three different fluids under Earth's gravity and microgravity conditions are plotted in Fig. 3 and Fig. 4. The variable π and Bo_{chf} exhibit a strong approximate power law correlation. This relationship can be approximated by Eq. (9), effectively providing a simplified dimensionless predictive relationship.

$$\log_{10}\left(Bo_{\mathrm{chf}}\right)=3.20\times\log_{10}(\pi)-0.56 \tag{9}$$

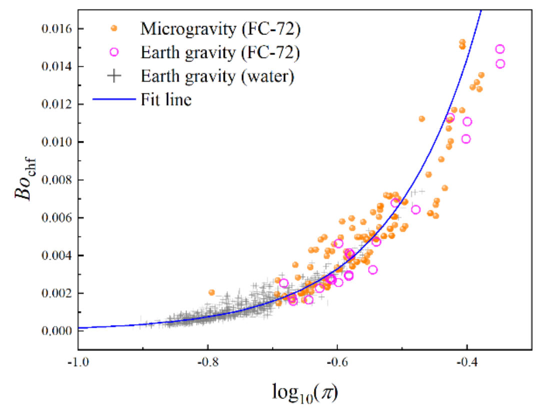

Fig 3 Correlation between $\log_{10}(\pi)$ and the Bo_{chf}

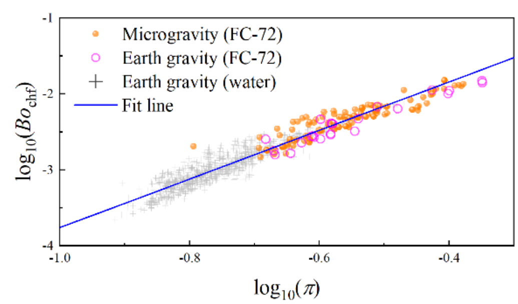

Fig 4 Power law relationship between π and the Bo_{chf}

3.2 *Decomposition based on standard dimensionless numbers*

Although the data-driven approach identified a dominant dimensionless number as shown in Eq. (8), its physical meaning remains unclear. Therefore, this section uses a set of easily interpretable standard dimensionless numbers to decompose the obtained π. The selected dimensionless numbers are listed in Table 2. The criteria for selecting this set of dimensionless numbers include: (1) The 10 dimensionless numbers are mutually exclusive; none can be expressed as a combination of the others. Non-compliance with this principle would not yield a definitive solution when decomposing dimensionless numbers, but merely an approximate least squares solution. To adhere to this requirement, after the inclusion of common dimensionless numbers, unique ones like *KR*, independent of other numbers, were also devised. (2) The power exponents of these numbers are integers, and their exponent vectors are as simplified as possible.

Table 2 Selected standard dimensionless numbers

Dimensionless number	Function
Geometric length ratio	$LR = \frac{L_h}{d}, LR_d = \frac{d_h}{d}$
Density ratio	$DR_{gf} = \frac{\rho_g}{\rho_f}, DR_{df} = \frac{\Delta\rho}{\rho_f}$
Weber number	$We = \frac{G^2 d}{\sigma\rho_f}$
Reynolds number	$Re = \frac{Gd}{\mu_f}$
Prandtl number	$Pr = \frac{\mu_f}{\rho_f \alpha_f}$
Equivalent inlet quality	$1 - x_{in} = \frac{\Delta h}{h_{fg}}$
Bond number	$Bd = \frac{g\Delta\rho d^2}{\sigma}$
Kinetic energy ratio number	$KR = \frac{G^2}{\rho_f^2 h_{fg}}$

Based on the aforementioned dimensionless numbers with clear physical meanings, the following result is obtained:

$$\pi = \frac{LR^{0.12} LR_h^{0.07} DR_{gf}^{0.10} Re^{0.40} Pr^{0.38} (1-x)^{0.40} Bd^{0.01} KR^{0.16}}{DR_{df}^{0.27} We^{0.47}} \tag{10}$$

Combining Eq. (9) and Eq. (10), Bo_{chf} is approximately proportional to $Bd^{0.032}$. Therefore, as the gravitational acceleration *g* decreases, the boiling number Bo also decreases, indicating that the CHF value decreases, which is consistent with existing experimental observations. Additionally, the Weber number We, representing two-phase instability, is negatively correlated with Bo_{chf}, aligning with previous fundamental studies. The inlet thermodynamic quality (x) is negatively correlated with Bo, indicating that a higher degree of subcooling at the inlet results in a lower Bo_{chf}.

3.3 Comparison with existing correlations

The simplified relationship derived from the data-driven dimensional analysis is given by Eq. (11). Its applicability is limited to a conservatively defined range of validated dimensionless numbers. This predictive model is used for comparative study against the three best correlation relationships for CHF under varying gravity conditions proposed by Madawar et al. These relationships are listed in Table 3, with equations referenced therein. The specific metrics used for evaluation are the Mean Absolute Error (MAE), Mean Absolute Percentage Error (MAPE), and the coefficient of determination (R^2), calculated over a total of 1597 data points, including both Earth's gravity and microgravity data. The formulas for these metrics are given in Eq. (12).

$$\pi = \frac{LR^{0.12} LR_h^{0.07} DR_{gf}^{0.10} Re^{0.40} Pr^{0.38} (1-x)^{0.40} Bd^{0.01} KR^{0.16}}{DR_{df}^{0.27} We^{0.47}}$$
$$\log_{10}(Bo_{chf}) = 3.20 \log_{10}(\pi) - 0.56 \tag{11}$$
$$-0.92 \le \pi \le -0.35$$

$$MAPE = \frac{100\%}{N} \times \sum_{i=1}^{N} \frac{|y_{pre,i} - y_{true,i}|}{y_{true,i}} \tag{12}$$
$$MAE = \frac{1}{N} \times \sum_{i=1}^{N} |y_{pre,i} - y_{true,i}|$$
$$R^2 = 1 - \frac{\sum_{i=1}^{N} (y_{pre,i} - y_{true,i})^2}{\sum_{i=1}^{N} (y_{true,i} - y_{mean})^2}$$

Table 3 Prediction results of compared correlations

Source (year)	*MAE*	*MAPE*	R^2
Tso et al. [22] (2000)	0.105	> 100%	< 0
Tibiriçá et al. [23] (2012)	0.0019	38.35%	0.33
Darges et al. [24] (2022)	0.00099	26.05%	0.82
Present work	0.00028	17.61%	0.91

According to Table 3, the present relationship yields more accurate predictions on a dataset comprising water and FC-72 under both microgravity and Earth's gravity conditions compared to previous works. This demonstrates that the dimensionless number π derived from the data-driven algorithm has strong representation capabilities for CHF under varying gravity conditions.

4. RESULTS

The present work introduces a data-driven dimensional analysis method based on neural networks and Buckingham's theorem, applied to predict CHF in vertical tube flow boiling under varying gravity conditions. The following key findings were obtained:

(1) A new dimensionless number π was identified, which has a strong influence on the boiling number Bo_{chf}. This dimensionless number exhibits a positive exponential scaling relationship with Bo_{chf}.

(2) The dimensionless number π was decomposed using a series of standard dimensionless numbers to make the expression interpretable.

(3) Based on the newly identified dimensionless number, a simplified predictive relationship was constructed. Comparison results show that the prediction accuracy of the new model surpasses that of previous correlation relationships, indicating that the feature quantities discovered through data-driven methods can effectively describe CHF in vertical tube flow boiling under varying gravity conditions.

The obtained correlation can be applied to predict flow boiling CHF under varying gravity conditions, such as microgravity in space, lunar gravity, and Martian gravity, holding potential value for energy management in deep space exploration.

ACKNOWLEDGEMENT

This work was supported by National Key R&D Program of China (Grant No.2023YFB4102205), Innovation Capability Support Program of Shaanxi (Program No.2023-CX-TD-18) and Innovative Scientific Program of CNNC.

REFERENCE

[1] Meyer ML, Hartwig JW, Sutherlin SG, Colozza AJ. Recent concept study for cryogenic fluid management to support opposition class crewed missions to Mars. Cryogenics. 2023;129.

[2] Liu Y, Liu W, Gu L, Shan J, Zhang L, Su X. Existing DNB-type CHF mechanistic models and relations with visualized experiments in forced convective flow boiling: A review. Progress in Nuclear Energy. 2022;148.

[3] Hall DD, Mudawar I. Critical heat flux (CHF) for water flow in tubes—II. International Journal of Heat and Mass Transfer. 2000;43:2605-40.

[4] Patricio F. Mendez TWE. The Matrix of Coefficients in Order of Magnitude Scaling. 2001.

[5] Constantine PG, del Rosario Z, Iaccarino G. Data-driven dimensional analysis: algorithms for unique and relevant dimensionless groups. arXiv preprint arXiv:170804303. 2017.

[6] Jofre L, del Rosario ZR, Iaccarino G. Data-driven dimensional analysis of heat transfer in irradiated particle-laden turbulent flow. International Journal of Multiphase Flow. 2020;125.

[7] Hang N, Wang Z, Liu M. A novel data-driven dimensional analysis framework for predicting melt pool morphology and porosity evolution in powder bed fusion. Journal of Materials Processing Technology. 2023;315.

[8] Xu Z, Zhang X, Wang S, He G. Artificial neural network based response surface for data-driven dimensional analysis. Journal of Computational Physics. 2022;459.

[9] Zhang L, Xu Z, Wang S, He G. Clustering dimensionless learning for multiple-physical-regime systems. Computer Methods in Applied Mechanics and Engineering. 2024;420.

[10] Mudawar I, Darges SJ, Devahdhanush VS. Parametric experimental trends, interfacial behavior, correlation assessment, and interfacial lift-off model predictions of critical heat flux for microgravity flow boiling with subcooled inlet conditions – Experiments onboard the International Space Station. International Journal of Heat and Mass Transfer. 2023;213.

[11] Mudawar I, Devahdhanush VS, Darges SJ, Hasan MM, Nahra HK, Balasubramaniam R, et al. Effects of heating configuration and operating parameters on heat transfer and interfacial physics of microgravity flow boiling with subcooled inlet conditions – Experiments onboard the International Space Station. International Journal of Heat and Mass Transfer. 2023;217.

[12] Mudawar I, Devahdhanush VS, Darges SJ, Hasan MM, Nahra HK, Balasubramaniam R, et al. Heat transfer and interfacial flow physics of microgravity flow boiling in single-side-heated rectangular channel with subcooled inlet conditions – Experiments onboard the International Space Station. International Journal of Heat and Mass Transfer. 2023;207.

[13] Mudawar I, Devahdhanush VS, Darges SJ, Hasan MM, Nahra HK, Balasubramaniam R, et al. Microgravity flow boiling experiments with liquid-vapor mixture inlet onboard the International Space Station. International Journal of Heat and Mass Transfer. 2024;224.

[14] Zhao X, Shirvan K, Salko RK, Guo F. On the prediction of critical heat flux using a physics-informed machine learning-aided framework. Applied Thermal Engineering. 2020;164.

[15] O'Neill LE, Mudawar I, Hasan MM, Nahra HK, Balasubramaniam R, Hall NR, et al. Experimental investigation into the impact of density wave oscillations on flow boiling system dynamic behavior and stability. Int J Heat Mass Transf. 2018;120:144-66.

[16] Darges SJ, Devahdhanush VS, Mudawar I, Nahra HK, Balasubramaniam R, Hasan MM, et al. Experimental results and interfacial lift-off model predictions of critical heat flux for flow boiling with subcooled inlet conditions – In preparation for experiments onboard the International Space Station. International Journal of Heat and Mass Transfer. 2022;183.

[17] Devahdhanush VS, Darges SJ, Mudawar I, Nahra HK, Balasubramaniam R, Hasan MM, et al. Flow visualization, heat transfer, and critical heat flux of flow boiling in Earth gravity with saturated liquid-vapor mixture inlet conditions – In preparation for experiments onboard the International Space Station. International Journal of Heat and Mass Transfer. 2022;192.

[18] Devahdhanush VS, Mudawar I, Nahra HK, Balasubramaniam R, Hasan MM, Mackey JR. Experimental heat transfer results and flow visualization of vertical upflow boiling in Earth gravity with subcooled inlet conditions – In preparation for experiments onboard the International Space

Station. International Journal of Heat and Mass Transfer. 2022;188.
[19] Yang K, Liang Z, Xu B, Hou Z, Wang H. Data-driven dimensional analysis of critical heat flux in subcooled vertical flow: A two-stage machine learning approach. Applied Thermal Engineering. 2024;248.
[20] Hendrycks D, Gimpel K. Gaussian error linear units (gelus). arXiv preprint arXiv:160608415. 2016.
[21] Kingma DP, Ba J. Adam: A method for stochastic optimization. arXiv preprint arXiv:14126980. 2014.
[22] Tso CP, Tou KW, Xu GP. Flow boiling critical heat flux of FC-72 from flush-mounted and protruded simulated chips in a vertical rectangular channel. International Journal of Multiphase Flow. 2000;26:351-65.
[23] Tibiriçá CB, Ribatski G, Thome JR. Saturated flow boiling heat transfer and critical heat flux in small horizontal flattened tubes. International Journal of Heat and Mass Transfer. 2012;55:7873-83.
[24] Darges SJ, Devahdhanush VS, Mudawar I. Assessment and development of flow boiling critical heat flux correlations for partially heated rectangular channels in different gravitational environments. International Journal of Heat and Mass Transfer. 2022;196.